IEEE Transactions on Automation Science and Engineering (T-ASE) paper, presented at ICRA 2026, Vienna, Austria.
Cite as T-ASE paper.

Curvature-Based Continuous Steering of Stiffness-Dominant Concentric Tube Robots

Luhao Xie, Lifeng Zhu, *Member, IEEE*, Xiaoliang Jin, *Member, IEEE*, and Aiguo Song, *Senior Member, IEEE*

***Abstract*—Existing works on controlling a concentric tube robot (CTR) mostly focus on the trajectory of its tip position or pose. In order to safely send CTRs in a confined lumen space, we propose to continuously steer the CTRs so that its entire shape will always attempt to approximate target curves over time. We focus on stiffness-dominant CTRs. Considering the differential geometry of such CTR shapes, we propose to work on the curvature domain to reduce the computational cost in searching the configuration of the CTRs. With our formulation, we model the curvature control of the CTR to find the optimal translation of each tube and then search for the rotation of the tubes to fit the target shapes. We demonstrate our method using sets of different target paths. The computational time per frame, ranging between 0.1 to 0.3 seconds across all experiments, highlights the efficiency of our approach in aligning the complete shape of the CTR with specified paths. Notably, for time-varying trajectories that could be reproduced by the CTR with its maximum deployment length reaching 150 mm, the root mean square error and median error were 0.98mm and 0.46mm, respectively.**

***Note to Practitioners*—This paper presents a novel approach for controlling stiffness-dominant CTRs, such that their entire shape consistently attempts to approximate target curves over time. This is crucial for applications such as navigation in confined anatomical spaces. Considering the differential geometry of these CTR shapes, we propose operating in the curvature domain. We model the curvature control of the CTR to determine the optimal translation for each segment, followed by searching for the rotation of the segments to fit the target shape. Our method avoids costly and computationally intensive full morphology evaluations while also achieving superior control accuracy, making it feasible for practical use in robotic surgery. In fact, this solution could be implemented in robot-assisted minimally invasive surgical platforms. Future work could explore adaptive modeling to address more complex clinical conditions, such as torsional deformations or variable tissue stiffness, or incorporate shape sensing for closed-loop control.**

Index Terms—**Concentric tube robots, curvature based, continuous steering.**

I. Introduction

A CONCENTRIC tube robot (CTR) is a type of continuum robot characterized by a nested assembly of pre-curved, elastic tubes [1]. By sliding or rotating these tubes relative to one another, a CTR can continuously form shape-changing curves, enabling it to approximate desired freeform trajectories even within confined spaces [2]. This capability positions CTRs as promising tools in the field of minimally invasive surgery, particularly for reaching target lesions along pre-planned freeform surgical paths [3].

In existing research on the control of CTRs, the inverse kinematics of the distal end—i.e., the control of the tip of the thinnest tube—has been extensively studied [4], [5], [6]. However, when the focus is exclusively on the motion state of the end-effector trajectory without considering the overall shape of the concentric tubes, unintended collisions can occur between the CTR body segments and surrounding tissues during traversal through anatomical passages. Such collisions may lead to potential injuries and adversely impact the control and effectiveness of the CTR. Consequently, to guide CTRs along freeform surgical paths toward desired regions, precise and continuous control of the entire shape of the CTR becomes essential in these scenarios.

Most existing works focus on the control of the end effector. To the best of our knowledge, the shape control of the entire CTR was first studied in 2022 [7]. Liang et al. developed S2J-IK, where the kinematics of the CTR were learned from captured data, and they proposed using a neural network as a surrogate model to solve for the inverse kinematics of the CTR, considering the entire shape of the target. However, this method cannot be directly applied to the continuous steering of CTRs. Because S2J-IK controls the CTR step by step, it does not account for the temporal continuity of control, which may result in abrupt changes in the control signal, leading to unstable motion of the CTR. Another challenge in continuous steering of CTRs is the computational cost. A fast computational method is required to continuously update the control signal, allowing the robot to adjust its shape according to time-varying desired paths. However, existing methods for comparing the shape of CTRs are computationally expensive, making the inverse problem in CTR control costly.

Received 11 December 2024; revised 10 March 2025; accepted 11 May 2025. Date of publication 16 May 2025; date of current version 28 May 2025. This article was recommended for publication by Associate Editor C. Dai and Editor H. Moon upon evaluation of the reviewers' comments. This work was supported in part by NSFC under Grant 92148205 and Grant 62133009, in part by the Natural Science Foundation of Jiangsu Province Major Project under Grant BK20232008, in part by Jiangsu Key Research and Development Plan under Grant BE2023023-4, in part by the Joint Fund Project under Grant 8091B042206, and in part by the Fundamental Research Funds for the Central Universities. *(Corresponding author: Lifeng Zhu.)*

The authors are with the State Key Laboratory of Digital Medical Engineering, Jiangsu Key Laboratory of Robot Sensing and Control, School of Instrument Science and Engineering, Southeast University, Nanjing 210096, China (e-mail: lfzhulf@gmail.com).

This article has supplementary downloadable material available at https://doi.org/10.1109/TASE.2025.3570861, provided by the authors.

Digital Object Identifier 10.1109/TASE.2025.3570861

IEEE Transactions on Automation Science and Engineering (T-ASE) paper, presented at ICRA 2026, Vienna, Austria.

An earlier strategy called "follow-the-leader" presents a viable solution for controlling the entire deployment process, as it ensures the robot deploys in such a way that the curved shape of its shaft remains unaltered as the tip progresses forward [8], [9], [10]. However, due to the limited motion space of the CTR, the robot is typically unable to perfectly follow any specified curved path. Existing research assumes that the paths to be followed are characterized by constant curvature or helical curves, or approximates the target path using these curves by designing appropriate pre-curved segments [11], [12], [13]. We note that the follow-the-leader mode may over-constrain the motion of CTRs. Instead, we directly fit time-varying paths produced by the CTR to approximate the desired path.

In this work, our focus is on the continuous steering of stiffness-dominant CTRs. To develop an efficient method for continuously controlling the CTR, we propose that it is unnecessary to evaluate the entire shape of the stiffness-dominant CTRs. Instead, by leveraging the characteristics of the dominant stiffness model, we focus on the curvature space. Given the known curvature and the rest shape of the tubes, the optimal control of the CTR can be simplified to enable fast continuous steering. We develop a curvature-based method and evaluate its performance with various target motion profiles. Experimental results demonstrate the efficacy of our method in continuously controlling the CTR. Furthermore, the computational time of our method, implemented in Python and run on a single CPU, is less than 0.3 seconds, highlighting its advantage in reducing computational costs.

Our contributions can be summarized as follows:

- The classical optimization-based shape-fitting planning algorithm has been extended to CTRs to enable precise tracking of arbitrary target paths.
- The cost function has been designed based on curvature optimization rather than position-based optimization, thereby simplifying the exploration of the configuration space for stiffness-dominant CTRs in continuous steering tasks.

A. Related Work

After the introduction of CTR in [14], [15], and [16], the community has solved the problems in the design and modeling of CTRs [17], [18], [19]. In addition to the design problem, various implementations of CTRs has also been proposed in the literature [20], [21], [22]. While complex models of general CTRs has been studied [2], the dominant stiffness model is generally preferred in the control of CTRs and found in many medical applications [23], [24], [25].

Traditional control methods for CTRs primarily focus on the desired end-effector motion, such as control methods based on the Jacobian of CTRs [26] or the Fourier series [2], [4]. The method based on Fourier series [4] approximates the inverse kinematics of the robot, trades off the generality and robustness for the computational performance. In general, the Jacobian-based method is fast enough for tracking the end-effector motion of CTRs and thus commonly used in numerous studies [27]. Regarding learning-based methods, a feedforward neural network with the target point's pose as input and configuration as output has been proposed [28]. Data-driven controllers [29] can directly learn complex dynamic models of CTR through Cartesian coordinates of the robot's tip position using electromagnetic trackers. However, the aforementioned methods only focus on controlling the tip of the CTR, without considering the overall shape of the robot.

Gilbert et al. [11] provided precise solutions for specific configurations of CTR in the context of the follow-the-leader motion and scrutinize the model-predicted deviation from ideal follow-the-leader behavior in approximate scenarios. Subsequently, Garriga-Casanovas and Baena [13] analyzed the complete shape space which could be planned as the follow-the-leader motion of CTRs. Xu et al. [30] improved computational performance by approximating follow-the-leader motion. As the target shape does not necessarily align with the follow-the-leader trajectories mentioned above, the shape control problem is still not perfectly solved by this deployment strategy.

Other than learning for the end-effector pose, Kuntz et al. [31] proposed a deep neural network-based approach for predicting the entire shape of CTRs. They utilized a convolutional neural network, taking the robot's configuration as input, and the output was a set of coefficients representing orthogonal polynomial basis functions that describe the shape of the CTR. With the learning-based approach, Liang et al. proposed to approximate the shape-to-joint inverse kinematic equations (S2J-IK) for CTRs, where the entire shape of the CTR is taken as the input for IK. In this case, the entire shape of CTRs can be controlled to fit target forms. The original S2J-IK finds the control signals of CTR by backpropagating the shape residuals with a pretrained neural network and is designed for fitting one specific curve. In this work, more than a static shape as the target, we plan to continuously control the CTR along time-varying curved trajectories. Besides, evaluating the entire shape with neural networks still demands a lot of computational resource and we expect a fast solution if we aim to continuously control the CTR.

II. Problem Definition

In this section, we first provide a formal definition of the continuous control problem associated with the CTRs, and in the subsequent section, we will present our proposed solution.

With the introduction of CTRs to medical applications, various CTR models have been developed, among which the dominant stiffness model is the most commonly utilized in practice [23], [24], [32]. Researchers have observed that if the stiffness ratio between consecutive tubes exceeds a certain threshold, stiffness dominance occurs, where the shape of the stiffer tube governs the configuration of the overlapping region. This phenomenon significantly simplifies the forward kinematics of CTRs. Additionally, it is typically assumed that the tubes are torsionally stiff, and torsional effects between the tubes are not incorporated. While this simplification may affect model accuracy, it greatly facilitates the control of CTRs, which is advantageous in practical applications.

The CTR system considered in this study consists of d individual tubes, each of which will be actively controlled. The

IEEE Transactions on Automation Science and Engineering (T-ASE) paper, presented at ICRA 2026, Vienna, Austria.

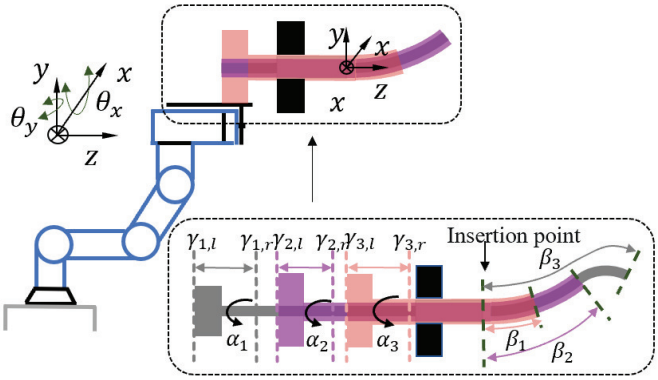

Fig. 1. The concentric tube robot and its configuration parameters.

first tube in the sequence is indexed as the outermost segment, while the last tube represents the innermost segment of the structure. To meet the requirements of the dominant stiffness model, the outermost tube is designed with a stiffness 6 to 8 times greater than that of the innermost tube, as referenced in [23]. For the ith tube, we define its total length as L_i, which is composed of two components: a straight segment of length $L_{s,i}$ and a curved segment of length $L_{c,i}$. The curved portion of each tube is designed to maintain a constant curvature, denoted as k_i. Each tube is independently controlled by two motors, which regulate its rotation, denoted by α_i, and its translation, denoted by β_i. In this work, β_i specifically represents the length of the segment of the ith tube that extends from the insertion point. Due to inherent physical constraints, the translation β_i is bounded by both upper and lower limits. These constraints stem from the design of the actuation mechanism, as well as the geometric properties of the straight and curved segments of each tube. These bounds ensure that each tube is able to either align with or extend beyond its adjacent outer tube. To represent these limits, we introduce the notation $\gamma_{i,r}$ and $\gamma_{i,l}$, which respectively denote the upper and lower bounds for the translation β_i, as illustrated in Fig. 1.

The curvature of a CTR, governed by the constant curvature principle, is characterized by the curvature vectors of individual segments, denoted as $\vec{k_i} = [k_{ix}, k_{iy}, k_{iz}]$ [16]. As we only consider torsionally stiff cases, k_{iz} can be ignored. Given the design parameters, the shape of the CTR can be formulated using the Arc Geometry method [33]

$$\mathbf{T}(s) = \begin{cases} \mathbf{T}_1(s), & s \in (0, \beta_1] \\ \prod_{i=1}^{m-1} \mathbf{T}_i(s_i)\mathbf{T}_m(s-\beta_{m-1}), & s \in (\beta_{m-1}, \beta_m], \\ & m = 2, 3, \ldots, d \\ s_i = \beta_i - \beta_{i-1}, \end{cases} \tag{1}$$

$$\beta_i \le \beta_{i+1}, \qquad i = 1, 2, \ldots, d-1 \tag{2}$$

$$\beta_i \in [\gamma_{i,l}, \gamma_{i,r}], \quad i = 1, 2, \ldots, d. \tag{3}$$

Here, $\beta_0 = 0$, and the parameters $\mathbf{T_i}$ and $\mathbf{T}_m$ can be obtained from [33] and [34]. Additionally, we define $k_i = \sqrt{k_{ix}^2 + k_{iy}^2}$. The selection of scalar curvature guarantees that the curvature values remain unaffected by rotation, thereby distinguishing rotation from extension. This aspect will be further elucidated in Section III.

The shape $\mathbf{C}_0(s)$ of the CTR as a parametric curve is then formed as $\mathbf{C}_0(s) = [\mathbf{T}_{1,4}(s), \mathbf{T}_{2,4}(s), \mathbf{T}_{3,4}(s)]^T$, which is the translational component in the homogeneous matrix $\mathbf{T}(s)$. In this context, where s denotes arc length, we subsequently normalize s in the following representations.

As CTR can be mounted on robot manipulators to extend its workspace [35], we further model the global orientation of the CTR into the system. Specifically, we assume that the insertion point is fixed and allow the CTR to globally rotate about the x-axis and y-axis of the coordinate system at the insertion point. The rotation angles are denoted by θ_x and θ_y, respectively. We do not model the global twist of the CTR again because the rotation of the first tube controls the global twist of the CTR. In this way, the curve of the CTR is output as

$$\mathbf{C}(s) = \mathbf{R}(\theta_x, \theta_y)\mathbf{C}_0(s), \tag{4}$$

where $\mathbf{R}(\theta_x, \theta_y)$ encodes the global rotation of the CTR. The configuration coordinate of the CTR can be parameterized as

$$q = (\alpha_1, \alpha_2, \ldots, \alpha_d, \beta_1, \beta_2, \ldots, \beta_d, \theta_x, \theta_y). \tag{5}$$

Because $\mathbf{C}_0(s)$ is a function of α_i, β_i, the curve $\mathbf{C}(s)$ is determined by q and we will write $\mathbf{C}(s|q)$ in the following when we consider the configuration coordinate q as a variable to control the shape $\mathbf{C}(s)$ of the CTR.

As for the continuous steering of the CTR, suppose the target shape of the CTR at the time t is given as $\bar{\mathbf{C}}(s,t)$, we take this as input and aim to solve the following problem

$$q(t) = argmin_{q(t)\in\mathbf{C}} d(\mathbf{C}(s|q(t)), \bar{\mathbf{C}}(s,t)) \tag{6}$$

to continuously command the CTR, so that the shape and pose of the CTR best align with the target time-varying shapes, where $d(\mathbf{C}(s|q(t)), \bar{\mathbf{C}}(s,t))$ measures the distance between the shape of the CTR $\mathbf{C}(s|q(t))$ and the target curve $\bar{\mathbf{C}}(s,t)$ at the time t. Note that previous works only consider the static shape $\mathbf{C}(s)$ or just the tip pose $\mathbf{C}(s=\beta_d)$ as the target. We hope to continuously control the CTR when it reaches a target region along a given path $\mathbf{C}(s)$. In this way, we may define the target shapes as

$$\bar{\mathbf{C}}(s,t) = \mathbf{C}(s), s \in [0, t/T], t \in (0, T], \tag{7}$$

so that the shape of the CTR will always try to approximate the target path during its process to reach the end at time T. Our objective diverges from the follow-the-leader approach as we aim not to fit a path $\mathbf{C}(s)$ that can be perfectly tracked by the follow-the-leader motion to the target path. Instead, we try to optimize the motion control to have the CTR align with the path as close as possible, so that the robot will 'softly' reproduce the follow-the-leader motion even if the path is not in the motion space of follow-the-leader strategy. Note that the parameter of the curve $\mathbf{C}(s)$ formed by CTR is $[0, \beta_d]$, which may be different from the parameter domain of $\bar{\mathbf{C}}(s,t)$. We, therefore, need to reparameterize these two curves into a common domain to facilitate the computation of the distance between two curves. For example, a trivial method is to use

IEEE Transactions on Automation Science and Engineering (T-ASE) paper, presented at ICRA 2026, Vienna, Austria.

TABLE I
DESIGN PARAMETERS OF THE CTR USED IN OUR WORK

Parameter			Set of tubes		
Term	Symbol	Unit	Tube1	Tube2	Tube3
Overall	L	$[mm]$	90	202	390
Straight	L_s	$[mm]$	50	107	150
Curvature	k	$[mm^{-1}]$	1/130	1/60	1/80
Outer Diameter	D_o	$[mm]$	5.7	3.7	2.1
Inner Diameter	D_i	$[mm]$	4.3	2.9	1.0

arc-length parameterization and scale the domain of each curve to $[0, 1]$, so that we may define

$$d(\mathbf{C}(s), \bar{\mathbf{C}}(s)) = \int_{s=0}^{s=1} \|\mathbf{C}(p(s)) - \bar{\mathbf{C}}(\bar{p}(s))\|^2 ds, \quad (8)$$

where $p(s)$ and $\bar{p}(s)$ are the reparameterization maps. However, as we only wish the shape of CTR align with the target curve and do not specify the correspondence of the curves, arc-length parameterization may not yield the best alignment and it is not trivial to search for a good reparameterization for comparing two curves [37], [38].

Before we proceed to introduce our method, we define a regularization term to the problem to show our preference on a smooth motion in continuously steering the CTR. Specifically, we further add a regularization term and the optimization problem turns to be

$$q(t) = argmin_{q(t)\in\mathcal{C}} d(\mathbf{C}(s|q(t)), \bar{\mathbf{C}}(s,t)) + \lambda\|\nabla q(t)\|^2, \quad (9)$$

where $\mathcal{C}$ is the constrained space defined in (2, 3) and $\|\nabla q(t)\|^2$ is the norm of the gradient of $q(t)$ w.r.t the time, which penalize large jumps of the configuration coordinate [38], where λ weights this regularization term. In the experiments presented in this paper, the specific value of λ will be provided in Section IV.

Without loss of generality, we will discuss our method with a CTR with three tubes. In our implementation, the design parameters of the CTR tested in this work are listed in Table I. The parameter settings in the table comply with the assumptions of the dominant stiffness model.

III. METHODOLOGY

The primary objective of this work is to enable CTRs to align with time-varying target shapes. While the robot's degrees of freedom may be limited, our goal is to find a solution that approximates the desired path as closely as possible. In this context, the CTR should be capable of autonomously deploying along a known trajectory, while simultaneously ensuring that its shape closely matches that of the target trajectory during operation. The problem can be framed as an optimization task, where the configuration coordinates q are determined by solving the optimization problem defined in (9). However, due to the inherent nonlinearity in the forward kinematics model described in (1) and the complexities involved in reparameterizing the two curves, a direct search for the configuration is computationally expensive. In this work, we focus on the dominant stiffness model, which simplifies the problem significantly. Specifically, we note that the shape formed by the CTR is a spatial curve characterized by piecewise constant curvature. The rotation α_i of each tube does not alter the curvature of the curve $\mathbf{C}(s)$, while the translation β_i only affects the jump points of the piecewise constant curvature. Leveraging the principles of differential geometry, we recognize that a spatial curve can be reconstructed from its differential quantities [40], [41]. Therefore, instead of focusing on reparameterization or calculating the integral in the objective defined in (8), we propose fitting the target shape in the differential domain. In this approach, the only parameter we need to focus on is the curvature, which is a piecewise constant function.

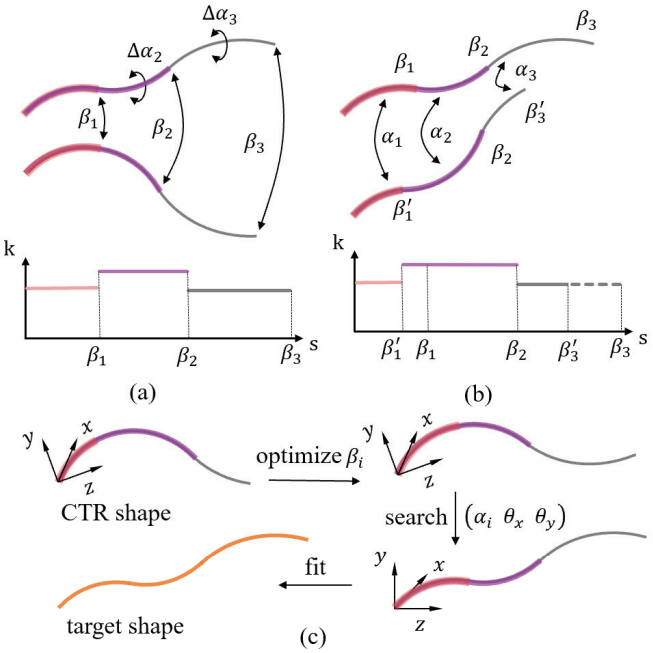

Fig. 2. The curvature of the stiffness-dominant CTR is not affected by the rotation of each tube (a) and only the jump point of the piecewise constant curvature is affected by the extension of each tube (b). Based on the observation, we first optimize for the tube extension to fit the curvature of target curve and then search for the tube rotation (c).

The computational pipeline for our model is depicted in Fig. 2. In the first step, we optimize the intrinsic shape segments defined by the tube extensions $(\beta_1, \beta_2, \beta_3)$ based on the curvature information. Subsequently, we search for the extrinsic orientation, controlled by $(\alpha_1, \alpha_2, \alpha_3, \theta_x, \theta_y)$, in order to align the spatial points with the target trajectory.

A. From Curvature to Tube Extensions

We will work on the curvature space to solve for the tube extension controls $(\beta_1, \beta_2, \beta_3)$. As depicted in Fig. 2(a), according to the dominant stiffness model, irrespective of the variations in rotation $(\alpha_1, \alpha_2, \alpha_3)$, the curvature of the shape $\mathbf{C}(s)$ formed by CTR remains a piecewise constant function, under the assumption that we only deploy the curved parts of each tube

$$k(s) = k_i, s \in [\beta_{i-1}, \beta_i],$$

IEEE Transactions on Automation Science and Engineering (T-ASE) paper, presented at ICRA 2026, Vienna, Austria.

where k_i is the curvature of the ith tube. If $\mathbf{C}(s)$ should match with a target shape $\bar{\mathbf{C}}(s)$, its curvature $k(s)$ should also align with the curvature of the target shape. Note that the translation β_i controls the extension of the ith tube, which is right the jump point of the piecewise constant curvature using the arc-length parameterization. We, therefore, aim to optimize β_i to make the piecewise constant curvature as close as possible to the curvature of the target shape

$$(\hat{\beta}_1, \hat{\beta}_2, \hat{\beta}_3) = \text{argmin}_{\beta_i} d(k(s|\beta_1, \beta_2, \beta_3), \bar{k}(s)), \tag{10}$$

where $k(s) = k_i$ for $s \in (\beta_{i-1}, \beta_i]$ and $\beta_0 = 0$. Suppose the parameter domain of the target shape $\bar{\mathbf{C}}(s)$ is $[0, L]$, we uniform the parameter domain of the target shape with a factor β_3/L. In this case, the tip of the CTR is defined to correspond to the end of the target shape. Therefore, the optimization problem turns to be

$$(\hat{\beta}_1, \hat{\beta}_2, \hat{\beta}_3) = \text{argmin}_{\beta_i} \sum_{i=1}^{3} \int_{\beta_{i-1}}^{\beta_i} (k_i - \bar{k}(s \cdot L/\beta_3))^2 ds. \tag{11}$$

We optimize (11) subject to the constraints defined in (2, 3) to make sure that the optimized control parameter β_i is physically valid for the CTR. Considering the temporal consistency of the control, suppose the translation of the ith tube at the last time step is $\beta_i^{(0)}$, we initialize $\beta_i = \beta_i^{(0)}$ and also add a regularization term $\sum_{i=1}^{3}(\beta_i - \beta_i^{(0)})^2$ into the above optimization problem to enhance the smoothness of the control.

To address the aforementioned constrained nonlinear optimization problem, the L-BFGS-B (Limited-memory Broyden-Fletcher-Goldfarb-Shanno with Bounds) solver is utilized in our implementation. We discretize the integral by uniformly sampling n points on the parametric domain and add the corresponding difference of the curvature on each sampled point. The curvature of the target shape can be analytically computed using its definition in differential geometry if the target shape is given as a parametric curve [41].

B. Tube Rotation Computation

Having obtained the tube extensions $\hat{\beta}_i$, we are ready to solve for the tube rotation controls $(\hat{\alpha}_1, \hat{\alpha}_2, \hat{\alpha}_3, \hat{\theta}_x, \hat{\theta}_y)$ by optimizing

$$\min d(\mathbf{C}(s|\alpha_1, \alpha_2, \alpha_3, \hat{\beta}_1, \hat{\beta}_2, \hat{\beta}_3, \theta_x, \theta_y), \bar{\mathbf{C}}(s)). \tag{12}$$

Similar to the computation of tube extension, we take the temporal consistency into consideration, initialize $\theta_x = \theta_x^{(0)}, \theta_y = \theta_y^{(0)}, \alpha_i = \alpha_i^{(0)}, i = 1, 2, 3$ to be the rotation angles at the last time step $(\theta_x^{(0)}, \theta_y^{(0)}, \alpha_1^{(0)}, \alpha_2^{(0)}, \alpha_3^{(0)})$ and add a regularization term $\sum_{i=1}^{3}(\alpha_i - \alpha_i^{(0)})^2 + (\theta_x - \theta_x^{(0)})^2 + (\theta_y - \theta_y^{(0)})^2$ to prefer a continuous control signal.

In the context of the spatial discretization of (12), and building upon the optimal extension parameter identified in Section III-A, we segment the target curve in a manner that best aligns with the tube segments. It is important to note that the optimal value of β_i directly corresponds to a point on the target curve, which is mapped to the position $s = \beta_i$ on the CTR shape. Under this shared parameterization, we are able to establish a robust correspondence between the CTR shape and the target curve. This approach obviates the need for uniformly resampling a large number of points along the curve, as would be the case when using arc-length parameterization to approximate the integral in (12). To evaluate the fitting performance, we conducted tests using varying numbers of sampled points, as demonstrated in Fig. 3. Based on the test results, we determined that a reasonable trade-off between accuracy and computational efficiency can be achieved by sampling only the endpoints and the midpoint of each segment in our implementation.

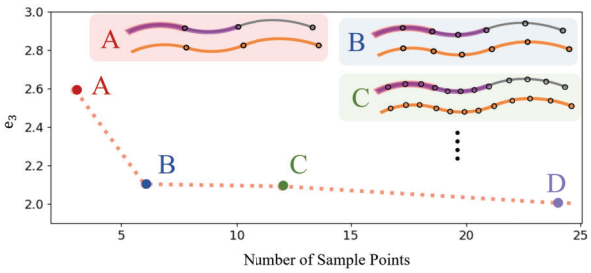

Fig. 3. The fitting error decreases with the increase of the sample points, while we find two point samples on a segment are sufficient for our method.

IV. Experimental Results

In this section, we evaluate the performance of our method by conducting experiments on a variety of target paths, which include primitive trajectories, freeform shapes, and time-varying trajectories. Additionally, we apply our method to control a CTR within a physical bronchial phantom model, demonstrating the practical significance of continuous steering for CTRs in real-world applications.

For all experimental setups, the weighting coefficient of the regularization term was set to 100 for our proposed method, and 500 for the baseline approach. The discrepancy in scale between the error terms in the curvature space and the Euclidean space necessitated different adjustments to the regularization weight, ensuring an appropriate balance between fidelity to the target path and the smoothness of the resulting trajectory. We implemented our proposed algorithm in Python and conducted the experiments on an Intel Core i5 processor, with a single core operating at 4.10 GHz. The computational time per frame for our method ranged from 0.1 to 0.3 seconds, while for the baseline approach, it ranged from 1.3 to 1.7 seconds. The specific average computational time per frame for each path is denoted as t_c and is presented in Table II.

Before showing the experimental results, we introduce the evaluation metrics here. We use the mean squared errors $e_1^j(s) = \sqrt{\left\|\mathbf{C}^j(s) - \bar{\mathbf{C}}^j(s)\right\|_2}$, $e_2^j = \sqrt{(1/\beta_3^j) \cdot \int_0^{\beta_3^j} e_1^j(s)^2 ds}$ where $e_1^j(s)$ represents the Euclidean distance between the points s on the CTR and the target trajectory at the jth time step, e_2^j represents the RMSE between all points on the entire shape at the jth time step. In addition, we also check the errors across the time range $E = (e_2^1, e_2^2, \ldots, e_2^{(T/\Delta t)})$ and use the RMSE $e_3 = \sqrt{\sum_j (e_2^j)^2/(T/\Delta t)}$ and the median of E denoted by e_4 to indicate the overall errors in the continuous steering process. All length units in this paper are in millimeters, and angular units are in radians, where Δt represents the time step.

IEEE Transactions on Automation Science and Engineering (T-ASE) paper, presented at ICRA 2026, Vienna, Austria.

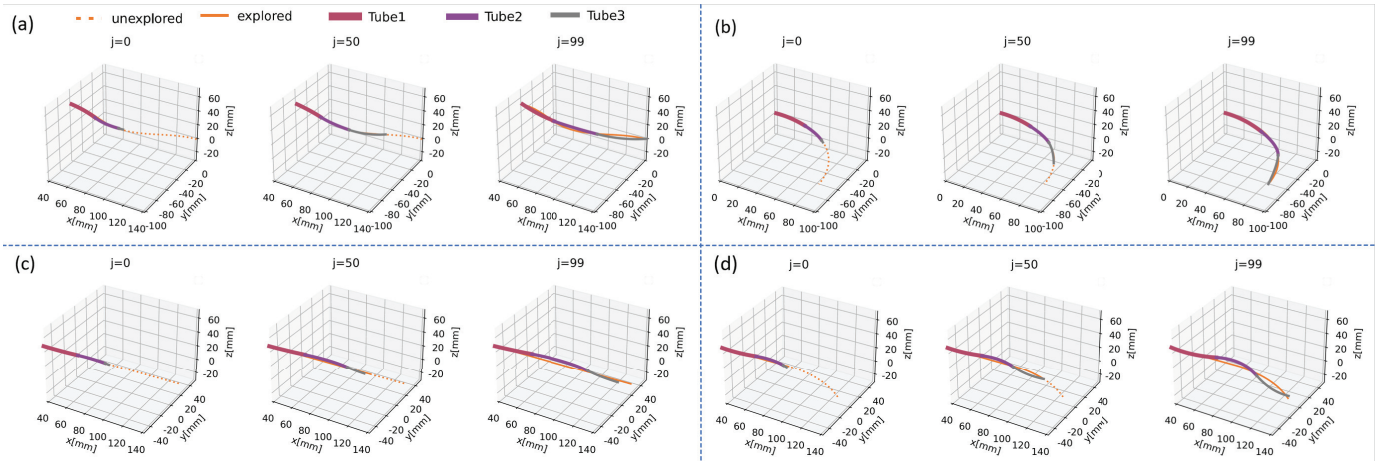

Fig. 4. Continuous path following results on primitive shapes of (a) a cosine-shaped curve, (b) an arc, (c) a straight line and (d) a straight line connected with an arc.

TABLE II
EVALUATION METRICS FOR DIFFERENT TARGET SHAPES

			cos	arc	line	line_arc	synthesis	bronchus
stiffness model	Ours	e_3	1.81	1.62	7.46	2.67	0.98	2.02
		e_4	1.67	1.36	4.84	1.88	0.46	1.93
	Baseline	e_3	1.84	1.81	7.58	2.84	3.28	2.71
		e_4	1.58	1.78	5.77	2.36	2.94	2.53
torsionally model	Ours	e_3	8.17	9.36	9.91	7.18	4.96	8.75
		e_4	6.43	7.51	8.02	5.31	2.90	7.17
	Baseline	e_3	9.92	10.46	11.19	10.40	7.35	9.31
		e_4	7.85	6.72	8.89	6.98	4.46	6.79
time	Ours	t_c	0.25	0.10	0.10	0.13	0.14	0.26
	Base line		1.63	1.34	1.31	1.39	1.43	1.67

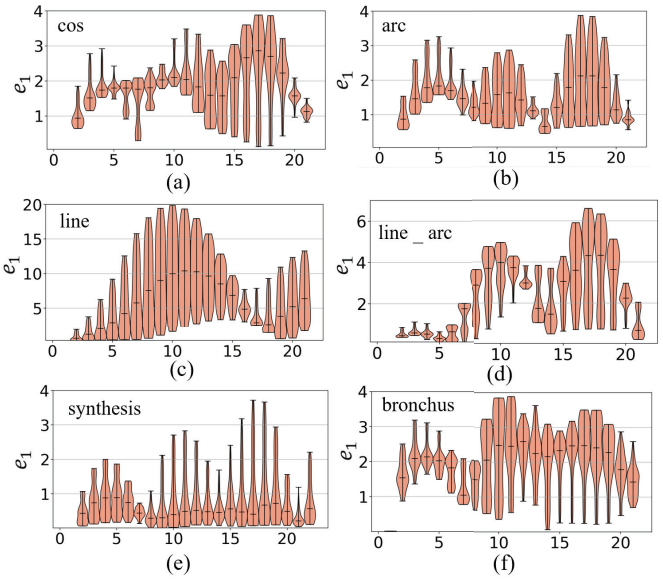

Fig. 5. The Violin plots of the distribution of point distance between the CTR shape and the target curve over time.

A. Continuous Path Following Experiments on Primitive Shapes

In this section, we conduct experiments to evaluate the performance of our method in the context of continuous path-following tasks using primitive shapes. According to the formulation in (7), the target shape evolves continuously along a given path $\mathbf{C}(s)$ during the test. Specifically, we selected four distinct path profiles, each representing a different primitive shape on the xy-plane. These include a cosine-shaped curve defined by $y = 10\cos(0.044x) - 10$, where $x \in [0, 45.45\pi]$; an arc described by $y = \sqrt{1 - x^2} - 100$, with $x \in [0, 100 \sin 1.5]$; a straight line given by $y = 0.02x$, for $x \in [0, 150]$; and a composite curve formed by connecting the second and third paths. For all these target curves, the parameterization is defined by $s = x$, ensuring a consistent reference for the path evolution.

We applied our algorithm to command the CTR to follow these paths, and several clips are shown in Fig. 4. The experimental results indicate that our method was successful in directing the CTR to traverse the paths, maintaining smooth continuous motion over time. To quantitatively assess the performance, we plotted the spatial distribution of the error measurement e_1^j at each time step for the four target paths in Fig. 5. Additionally, the overall errors e_3 and e_4 for the entire continuous deployment process are summarized in Table II. It is important to note that the target path may not always be a shape that can be perfectly reproduced by the CTR due to the inherent limitations of its design. For instance, since the CTR is constructed from three tubes, each having a constant curvature, it inherently cannot replicate a straight line. This limitation partially accounts for the relatively large errors observed when attempting to follow certain primitive curves, such as straight lines. Despite this constraint, our method demonstrates notable flexibility, as the CTR is still capable of continuously maneuvering along a path that approximates the straight line, as illustrated in Fig. 4(c).

To validate the advantages of our proposed curvature-based method, we conducted a comparative analysis with a baseline

IEEE Transactions on Automation Science and Engineering (T-ASE) paper, presented at ICRA 2026, Vienna, Austria.

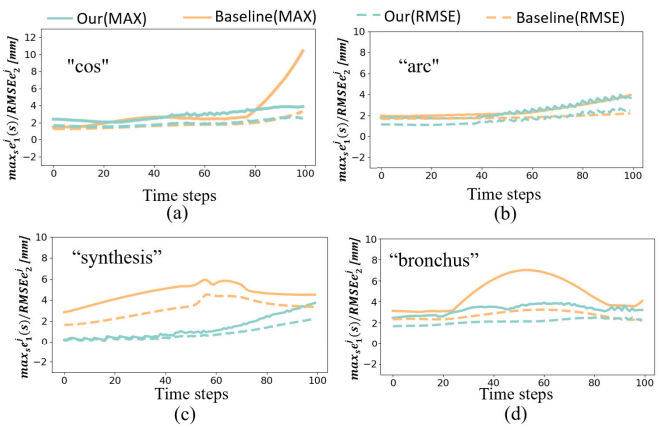

Fig. 6. The maximum and root mean square error distribution with the deployment of the CTR.

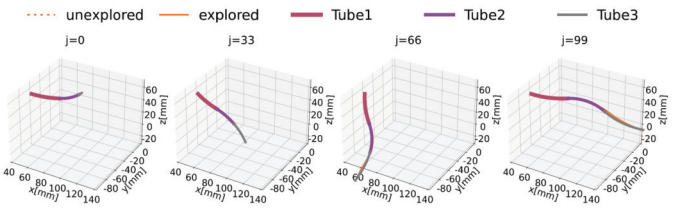

Fig. 7. Continuous steering results for time-varying target shapes.

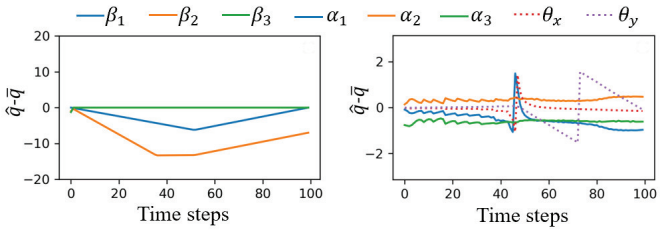

Fig. 8. The errors of the configuration coordinates for the synthesized time-varying targets.

approach that directly evaluates errors in the Euclidean space. Specifically, we implemented a Jacobian-based optimization framework as the reference, which minimizes (9) using the distance metric defined in (8) under the arc-length parameterization. Since this optimizer requires gradient information, we employed the L-BFGS-B algorithm, which is consistent with the approach used in our method. We subjected all four curves depicted in Fig. 4 to identical inputs and assessed their performance metrics for comparative analysis. The overall errors e_3 and e_4 are also detailed in Table II. Furthermore, we plotted the maximum error $max_s e_1^j(s)$ and the RMSE e_2^j at each time frame for both the cosine-shaped curve and the arc in Fig. 6(a) and (b). We found larger errors from the results of the baseline because the assumed arc-length parameterization may not be the optimum reparameterization for comparing the CTR shape and its target, while our method opt to search the extension β to better align the curves with optimizable parameterization. In particular, concerning the cosine-shaped curve, the baseline method demonstrated a noticeable escalation in error beyond 80 frames, whereas our approach does not exhibit such behavior. This observation suggests that baseline faltered in making optimal decisions when the deployment length of the CTR approached the operational boundary for challenging paths. Upon examining Fig. 6(b), it is apparent that for arc-shaped target trajectories, which were relatively easy to find solutions for, our method exhibited errors comparable to the baseline.

B. Experiments on Time-Varying Shapes

Then we experimented our method with a time-varying target $\bar{\mathbf{C}}(s,t)$. In this test, we generate time-varying trajectories that could be reproduced by the CTR. In this case, we could also evaluate our results with a ground-truth signal as the reference. Specifically, the test data were generated as $\bar{\mathbf{C}}(s,t) = \mathbf{C}(s|\bar{q}(t))$, where $\bar{q}(t) = (1-t)q_1 + tq_2$, in which we set $q_1 = (38, 70, 75, 0, 0, 0, 0, 0)$ and $q_2 = (50, 107, 150, \pi, \pi, \pi, \pi)$. We sampled T frames of the configuration coordinates and used forward kinematics ((1) and (4)) to generate the target time-varying shapes, with $\bar{q}(t)$ as the ground-truth of the control signal.

We plotted the results in Fig. 7. As shown in the figure, the CTR well aligned with the target time-varying shapes provided in this example. We also listed the statistics of the errors in Fig. 5(e) and Table II. Because the target time-varying shapes were within the workspace of the CTR, the errors were relatively small in this example. As we have the grouth-truth signal $\bar{q}(t)$ as the reference, we also plotted the errors in the configuration space $\hat{q}(t) - \bar{q}(t)$, where $\hat{q}(t)$ is obtained by our method, in Fig. 8. The errors in the configuration space also validated the efficacy of our method. We also noted that the errors in the configuration space were not perfectly close to zero, because our method also considered the smoothness regularization term and might still deviate the results. We also tested the baseline using time-varying trajectories and plotted the maximum error $max_s e_1^j(s)$ and the RMSE e_2^j at each time frame. The overall errors e_3 and e_4 are also provided in Table II. As illustrated in Fig. 6(c), the baseline method consistently exhibited significantly inferior performance compared to ours, suggesting that our method demonstrated its adaptability to trajectories with large-scale variations.

C. Experiments on Freeform Shapes

Finally, we applied our method to control a freeform shape extracted from a bronchial model to assess its performance in a realistic scenario. The method described in [42] was employed to extract the curved skeleton of the bronchial model, which, unlike a well-designed curve, does not perfectly fit within the motion space of the CTR. This makes the skeleton particularly suitable for evaluating the effectiveness of our approach in dealing with 'organic' curves that are not explicitly designed for CTR motion. In this experiment, we used the curved skeleton as the target freeform path for the CTR to follow. Our method was applied to continuously steer the CTR along the curved skeleton, which approximated the centerline of the bronchial lumen. In this scenario, as the CTR attempted to move its tip toward the target, it was also required to maintain

IEEE Transactions on Automation Science and Engineering (T-ASE) paper, presented at ICRA 2026, Vienna, Austria.

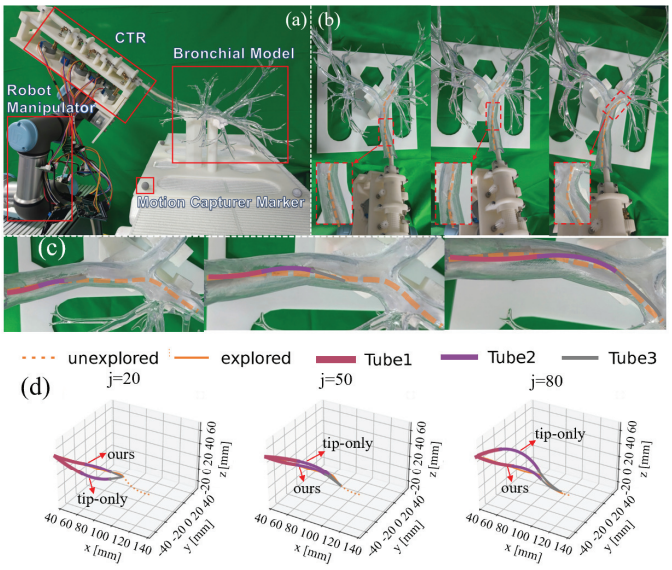

Fig. 9. (a) Real-world experiment on a physical phantom. (b) The CTR walks inside the bronchial model with its entire shape aligned with the centerline. (c) A zoomed-in view for the comparison between experimental and simulation results. (d) Continuous path following results on a freeform curve extracted from a bronchus path. Only controlling the tip trajectory may result in bad alignment of the CTR to the path.

a consistent distance from the bronchial wall, ensuring that its entire shape adapted to the surrounding environment. The results obtained from our method are presented in Fig. 9(d). It is evident that the CTR made considerable efforts to keep its shape aligned with the target freeform curve throughout the operation. Additionally, the errors associated with this alignment are provided in the violin plot shown in Fig. 5(f) and Table II, further demonstrating the accuracy and efficacy of our approach.

To further evaluate the performance of our method, we compared the results with those obtained by controlling only the end-effector's position, as shown in Fig. 9(d). In this comparison, we employed a traditional Jacobian-based method [26] to control the tip of the CTR, steering it along the freeform shape. The comparison revealed that while the tip of the CTR, under this approach, was able to closely track the target freeform path, several segments of its entire shape were noticeably misaligned with the curved skeleton. This misalignment indicates a potential issue with overall shape coherence when using the tip-only control strategy. In contrast, our proposed method yielded a better overall shape alignment, where the entire shape of the CTR followed the target freeform curve more consistently. This improved alignment makes our approach more suitable for medical applications, where safety and precise shape control are critical, ensuring that the CTR maintains a safe distance from surrounding tissue and accurately follows complex paths.

In addition to the primary evaluation, we further assessed the performance of the baseline method by comparing its results against the prescribed trajectories. The corresponding plots and data are presented in Fig. 6(d) and Table II. The results reveal that, during the initial 20 frames and the final 10 frames, both the baseline and our proposed approach exhibited similar levels of error. However, a notable discrepancy arose in the intermediate frames, where the target trajectory underwent significant curvature changes. In this range, our approach displayed superior adaptability, effectively adjusting to these variations and demonstrating improved performance in tracking the trajectory compared to the baseline.

We implemented the bronchial path derived from our simulation experiments in a real-world physical environment. The complete experimental setup is illustrated in Fig. 9(a), showcasing the physical deployment of the CTR. The CTR used in the physical experiments was designed with the same parameters as those in the simulation, ensuring consistency between the two environments. The concentric tubes themselves were fabricated using PolyCaprolactone (PCL) through 3D printing [22]. The actuation mechanism of the CTR incorporated a compact gear structure, as described in [20], which was also manufactured using 3D printing techniques. Six stepper motors were employed to actuate the CTR, with the motor commands being transmitted to the Robot Operating System (ROS) platform via an Arduino interface, facilitating seamless communication between the hardware and the control system. Additionally, a UR3 robotic arm was used to provide global rotation (θ_x, θ_y) for the CTR, ensuring precise control over the robot's orientation. Both the robotic manipulator and the stepper motors were controlled by commands issued from a single file in the ROS environment, ensuring synchronization of actions across the system for each frame of operation. To further simulate the bronchial path, a physical 3D model of the bronchial system was printed using the same mesh that was employed to extract the curved skeleton. After assembling the physical model, we calibrated the relative pose between the robotic manipulator and the bronchial model using an optical motion capture system (Nokov Mars2H).

Once the experimental environment was established, we proceeded by commanding the planned configuration coordinates to the CTR, and subsequently obtained the results depicted in Fig. 9(b). To facilitate a meaningful comparison between the performance of our method in the simulation and its deployment in a real-world physical environment, we overlaid the simulation results—highlighted with distinct strokes—on the captured real-world data shown in Fig. 9(c). As the CTR gradually advanced into the bronchial pathway, we observed that it consistently attempted to maintain its entire shape in alignment with the centerline of the bronchial model. Importantly, we did not impose rigid constraints to prevent contact between the CTR and the bronchial model. In certain extreme cases, mild contact with the inner wall may occur, and due to the elasticity of the concentric tubes, some yielding may take place. However, it is worth noting that, given our primary objective of ensuring the CTR's entire shape follows the curved skeleton, such extreme cases occurred infrequently during our testing.

V. Discussion

In this work, we fully exploit the feature of stiffness-dominant CTRs and propose to work on the curvature domain for continuously steering the CTR. Our idea may extend to

IEEE Transactions on Automation Science and Engineering (T-ASE) paper, presented at ICRA 2026, Vienna, Austria.

support general CTRs, as long as the curvature of the overlapping region of the tubes can be modeled either analytically or using learning-based models.

To more accurately assess the errors, we employed the torsionally compliant kinematics model [2], which is more precise yet complex, to simulate the forward motion when calculating e_3 and e_4 for all experiments. The results are presented in the lower lines of Table II. As we only substituted the complex model during the evaluation, rather than during the optimization process, the errors calculated after replacing the model are higher than the original ones. Our method tends to encounter relatively larger tracking errors when tasked with following the most challenging straight-line shape targets for pre-curved CTRs. In such scenarios, deployment is not advisable, and adjusting the design parameters of the CTRs is recommended to effectively mitigate these errors. However, from the results, we still found smaller errors of our method compared to the baseline. Therefore, considering the computational cost, we still use the simplified model during the optimization stage. In the rightmost plot of Fig 9(c), one can observe that the innermost tube may be affected by torsional effects, leading to discrepancies between the simulation results and real-world scenarios. Advanced models could mitigate such differences.

In this paper, our focus did not encompass hysteresis and snapping, phenomena associated with the sudden release of elastic energy accumulated due to the twisting of tubes. This phenomenon is indeed a challenging problem in CTR control and may lead to instability issues. In the future, we will explore the potential of employing a model capable of capturing both snapping and hysteresis for CTRs [43] in our method for addressing these issues.

In order to test the potential of our method to accommodate general CTR designs other than constant-curvature models, we preliminary experimented our solution for CTRs with variable-curvature segments, as shown in Fig. 10. In the experiment, the segments of the CTR were set as three different Euler curves [44], [45], while the target path is another Euler curve with different linearly-varying curvatures. We further provided another CTR design, with its three segments pre-stressed as a line segment, an arc and a Euler curve. Using the same target path in Fig. 10(a), we used our curvature-based model to control the CTR and found the robot well followed path with the new design, as shown in Fig. 10(b). From the results, it is evident that our method demonstrates its potential for generalization across various configurations of stiffness-dominant concentric tubes.

Our solution is essentially a model-based method. Although the data-driven method using machine learning may incorporate the fabrication errors, friction or other factors into the trained neural networks, we find the back-propagation process in search of the control parameters using neural networks does not guarantee the results to satisfy the hard constraints, e.g., the range of the β_i in (2, 3). Besides, the training process is also computional expensive and it is costly to collect sufficient data for the learning-based method. From the simulation results, we find the model-based method works well. Therefore, our

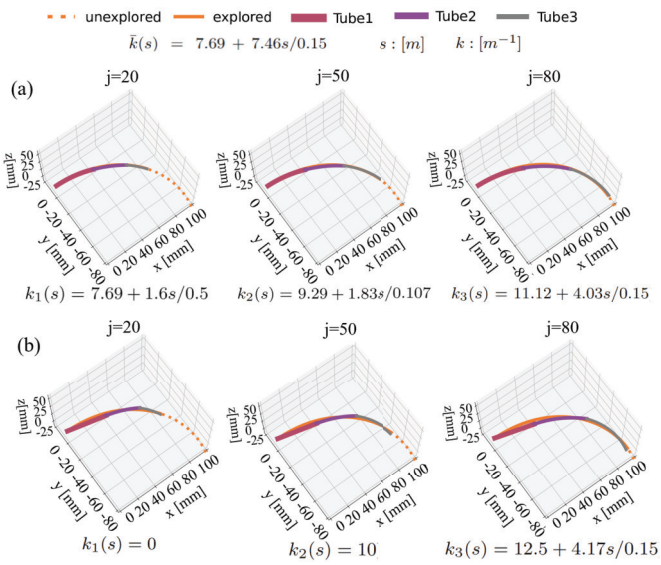

Fig. 10. Continuous trajectory tracking results concerning CTRs with variable-curvature tubes. We use $k_i(s)$ to represent the curvature of the ith tube and $\bar{k}(s)$ encodes the curvature distribution of the target path. The segments of the CTR were pre-stressed as (a) three different Euler curves and (b) a line segment, an arc and a Euler curve.

method is valuable if the robot is well calibrated or the sim2real process is appropriately modeled.

Limited by the degrees of freedom of CTRs, the continuous steering of CTRs will not produce good results if the target curves are far from the workspace spanned by the CTR design. Moreover, in a confined workspace, deviations of the robot's shape from its target trajectory may inevitably result in unintended contact with the surrounding walls. Consequently, the tube may conform to these contacts, leading to global deformation. Additionally, this work assumes that no external load is exerted on the robot. Under such conditions, the geometric model may become ineffective for control. This problem could be alleviated if we take the design problem of the CTR into consideration as one of our future works. We may simultaneously optimize the design parameters and the control parameters of the CTR for producing a better motion in complex confined space. The adoption of a more complex load model during the optimization process could also help mitigate this issue. Finally, the weighting coefficient of the regularization term can also influence the optimization results. When faced with more complex target paths, it may also require corresponding adjustment.

In our experiment, we implemented our method using python and experimented it on a single CPU. We get comparable performance with the latest work on shape control of CTR computed using GPU. In the future, we will develop our method with GPU implementations to further accelerate its performance. Furthermore, this is beneficial for our future endeavors, as the incorporation of more sophisticated models is anticipated to enhance accuracy, notwithstanding the concurrent rise in computational requirements. Besides, in combination with shape-sensing or positioning capabilities,

IEEE Transactions on Automation Science and Engineering (T-ASE) paper, presented at ICRA 2026, Vienna, Austria.

our method can be used to the online control of the CTR due to its fast performance, which is another potential direction for future work.

VI. Conclusion

In this work, we address the continuous steering problem for CTRs, which represents a more complex challenge compared to controlling only the tip of the CTR. While the computational cost is higher for continuous steering, this approach offers the advantage of providing more precise control over the entire shape of the robot. To facilitate the search for optimal control parameters, we propose a curvature-based solution tailored for stiffness-dominant CTRs. By formulating the control problem within the curvature space, we demonstrate that the configuration coordinates of the CTR can be efficiently optimized, leading to more effective steering strategies.

We validate the effectiveness of our approach through a series of experiments conducted on various sets of target trajectories. The results reveal the practical efficacy of our method, with the per-frame computational time ranging from 0.1 to 0.3 seconds across all experiments. For time-varying target trajectories, with the CTR's maximum deployment length reaching 150 mm, we achieve a root mean square error (RMSE) of 0.98 mm and a median error of 0.46 mm. These results highlight the accuracy and efficiency of our approach, even when dealing with dynamic target shapes.

As the first attempt to continuously steer concentric tube robots, our method opens up new possibilities for steering CTRs in a more flexible and dynamic manner. Moving forward, we plan to further explore efficient solutions for controlling CTRs in constrained environments. To quickly demonstrate the potential of our proposed method, we conduct preliminary experiments using a limited set of typical inputs. We also intend to extend our experiments to more diverse datasets in the future to fully assess the performance and robustness of the curvature-based approach.

References

[1] H. B. Gilbert, D. C. Rucker, and R. J. Webster, "Concentric tube robots: The state of the art and future directions," in *Proc. Robot. Res., 16th Int. Symp. ISRR*. Springer, Jan. 2016, pp. 253–269.

[2] P. E. Dupont, J. Lock, B. Itkowitz, and E. Butler, "Design and control of concentric-tube robots," *IEEE Trans. Robot.*, vol. 26, no. 2, pp. 209–225, Apr. 2010.

[3] J. Burgner-Kahrs, D. C. Rucker, and H. Choset, "Continuum robots for medical applications: A survey," *IEEE Trans. Robot.*, vol. 31, no. 6, pp. 1261–1280, Dec. 2015.

[4] P. E. Dupont, J. Lock, and B. Itkowitz, "Real-time position control of concentric tube robots," in *Proc. IEEE Int. Conf. Robot. Autom.*, May 2010, pp. 562–568.

[5] R. Xu, A. Asadian, S. F. Atashzar, and R. V. Patel, "Real-time trajectory tracking for externally loaded concentric-tube robots," in *Proc. IEEE Int. Conf. Robot. Autom. (ICRA)*, May 2014, pp. 4374–4379.

[6] M. Khadem, J. O'Neill, Z. Mitros, L. Da Cruz, and C. Bergeles, "Autonomous steering of concentric tube robots via nonlinear model predictive control," *IEEE Trans. Robot.*, vol. 36, no. 5, pp. 1595–1602, Oct. 2020.

[7] N. Liang, R. M. Grassmann, S. Lilge, and J. Burgner-Kahrs, "Learning-based inverse kinematics from shape as input for concentric tube continuum robots," in *Proc. IEEE Int. Conf. Robot. Autom. (ICRA)*, May 2021, pp. 1387–1393.

[8] E. Amanov, T.-D. Nguyen, and J. Burgner-Kahrs, "Tendon-driven continuum robots with extensible sections—A model-based evaluation of path-following motions," *Int. J. Robot. Res.*, vol. 40, no. 1, pp. 7–23, Jan. 2021.

[9] Y. Gao, K. Takagi, T. Kato, N. Shono, and N. Hata, "Continuum robot with follow-the-leader motion for endoscopic third ventriculostomy and tumor biopsy," *IEEE Trans. Biomed. Eng.*, vol. 67, no. 2, pp. 379–390, Feb. 2020.

[10] C. Girerd, A. V. Kudryavtsev, P. Rougeot, P. Renaud, K. Rabenorosoa, and B. Tamadazte, "SLAM-based follow-the-leader deployment of concentric tube robots," *IEEE Robot. Autom. Lett.*, vol. 5, no. 2, pp. 548–555, Apr. 2020.

[11] H. B. Gilbert, J. Neimat, and R. J. Webster, "Concentric tube robots as steerable needles: Achieving follow-the-leader deployment," *IEEE Trans. Robot.*, vol. 31, no. 2, pp. 246–258, Apr. 2015.

[12] C. Girerd, K. Rabenorosoa, P. Rougeot, and P. Renaud, "Towards optical biopsy of olfactory cells using concentric tube robots with follow-the-leader deployment," in *Proc. IEEE/RSJ Int. Conf. Intell. Robots Syst. (IROS)*, Sep. 2017, pp. 5661–5887.

[13] A. Garriga-Casanovas and F. Rodriguez y Baena, "Complete follow-the-leader kinematics using concentric tube robots," *Int. J. Robot. Res.*, vol. 37, no. 1, pp. 197–222, Jan. 2018.

[14] J. Furusho, T. Ono, R. Murai, T. Fujimoto, Y. Chiba, and H. Horio, "Development of a curved multi-tube (CMT) catheter for percutaneous umbilical blood sampling and control methods of CMT catheters for solid organs," in *Proc. IEEE Int. Conf. Mechatronics Autom.*, Jul. 2005, pp. 410–415.

[15] R. Webster, A. Okamura, and N. Cowan, "Toward active cannulas: Miniature snake-like surgical robots," in *Proc. IEEE/RSJ Int. Conf. Intell. Robots Syst.*, Oct. 2006, pp. 2857–2863.

[16] P. Sears and P. Dupont, "A steerable needle technology using curved concentric tubes," in *Proc. IEEE/RSJ Int. Conf. Intell. Robots Syst.*, Oct. 2006, pp. 2850–2856.

[17] D. C. Rucker, B. A. Jones, and R. J. Webster III, "A geometrically exact model for externally loaded concentric-tube continuum robots," *IEEE Trans. Robot.*, vol. 26, no. 5, pp. 769–780, May 2010.

[18] D. C. Rucker and R. J. Webster, "Computing Jacobians and compliance matrices for externally loaded continuum robots," in *Proc. IEEE Int. Conf. Robot. Autom.*, May 2011, pp. 945–950.

[19] C. Bedell, J. Lock, A. Gosline, and P. E. Dupont, "Design optimization of concentric tube robots based on task and anatomical constraints," in *Proc. IEEE Int. Conf. Robot. Autom.*, May 2011, pp. 398–403.

[20] C. Girerd and T. K. Morimoto, "Design and control of a hand-held concentric tube robot for minimally invasive surgery," *IEEE Trans. Robot.*, vol. 37, no. 4, pp. 1022–1038, Aug. 2021.

[21] T. K. Morimoto and A. M. Okamura, "Design of 3-D printed concentric tube robots," *IEEE Trans. Robot.*, vol. 32, no. 6, pp. 1419–1430, Dec. 2016.

[22] T. K. Morimoto, J. D. Greer, E. W. Hawkes, M. H. Hsieh, and A. M. Okamura, "Toward the design of personalized continuum surgical robots," *Ann. Biomed. Eng.*, vol. 46, no. 10, pp. 1522–1533, Oct. 2018.

[23] C. Bergeles, A. H. Gosline, N. V. Vasilyev, P. J. Codd, P. J. del Nido, and P. E. Dupont, "Concentric tube robot design and optimization based on task and anatomical constraints," *IEEE Trans. Robot.*, vol. 31, no. 1, pp. 67–84, Feb. 2015.

[24] T. Anor, J. R. Madsen, and P. Dupont, "Algorithms for design of continuum robots using the concentric tubes approach: A neurosurgical example," in *Proc. IEEE Int. Conf. Robot. Autom.*, May 2011, pp. 667–673.

[25] P. Sears and P. E. Dupont, "Inverse kinematics of concentric tube steerable needles," in *Proc. IEEE Int. Conf. Robot. Autom.*, Apr. 2007, pp. 1887–1892.

[26] R. Xu, A. Asadian, A. S. Naidu, and R. V. Patel, "Position control of concentric-tube continuum robots using a modified jacobian-based approach," in *Proc. IEEE Int. Conf. Robot. Autom.*, May 2013, pp. 5813–5818.

[27] S. Vougioukas, "Annual review of control, robotics, and autonomous systems," *Agricult. Robot.*, vol. 2, no. 1, pp. 365–392, 2019.

[28] R. Grassmann, V. Modes, and J. Burgner-Kahrs, "Learning the forward and inverse kinematics of a 6-DOF concentric tube continuum robot in SE(3)," in *Proc. IEEE/RSJ Int. Conf. Intell. Robots Syst. (IROS)*, Oct. 2018, 5125–5132.

[29] B. Thamo, D. Hanley, K. Dhaliwal, and M. Khadem, "Data-driven steering of concentric tube robots in unknown environments via dynamic mode decomposition," *IEEE Robot. Autom. Lett.*, vol. 8, no. 2, pp. 856–863, Feb. 2023.

IEEE Transactions on Automation Science and Engineering (T-ASE) paper, presented at ICRA 2026, Vienna, Austria.

[30] Y. Xu, C. Watson, J.-T. Lin, J. T. Hwang, and T. K. Morimoto, "Shape control of concentric tube robots via approximate follow-the-leader motion," *IEEE Robot. Autom. Lett.*, vol. 9, no. 8, pp. 7198–7205, Aug. 2024.
[31] A. Kuntz, A. Sethi, R. J. Webster, and R. Alterovitz, "Learning the complete shape of concentric tube robots," *IEEE Trans. Med. Robot. Bionics*, vol. 2, no. 2, pp. 140–147, May 2020.
[32] J. Burgner, P. J. Swaney, R. A. Lathrop, K. D. Weaver, and R. J. Webster, "Debulking from within: A robotic steerable cannula for intracerebral hemorrhage evacuation," *IEEE Trans. Biomed. Eng.*, vol. 60, no. 9, pp. 2567–2575, Sep. 2013.
[33] R. J. Webster III and B. A. Jones, "Design and kinematic modeling of constant curvature continuum robots: A review," *Int. J. Robot. Res.*, vol. 29, no. 13, pp. 1661–1683, 2010.
[34] G. S. Chirikjian and J. W. Burdick, "A modal approach to hyper-redundant manipulator kinematics," *IEEE Trans. Robot. Autom.*, vol. 10, no. 3, pp. 343–354, Jun. 1994.
[35] T. K. Morimoto, E. W. Hawkes, and A. M. Okamura, "Design of a compact actuation and control system for flexible medical robots," *IEEE Robot. Autom. Lett.*, vol. 2, no. 3, pp. 1579–1585, Jul. 2017.
[36] S. Cohen, G. Elber, and R. Bar-Yehuda, "Matching of freeform curves," *Computer-Aided Design*, vol. 29, no. 5, pp. 369–378, May 1997.
[37] P. Costantini, R. T. Farouki, C. Manni, and A. Sestini, "Computation of optimal composite re-parameterizations," *Comput. Aided Geometric Design*, vol. 18, no. 9, pp. 875–897, Nov. 2001.
[38] A. Aristidou, J. Lasenby, Y. Chrysanthou, and A. Shamir, "Inverse kinematics techniques in computer graphics: A survey," *Comput. Graph. Forum*, vol. 37, no. 6, pp. 35–58, Sep. 2018.
[39] M. Desbrun, E. Kanso, and Y. Tong, "Discrete differential forms for computational modeling," in *Proc. ACM SIGGRAPH Courses-SIGGRAPH*, 2005, p. 7.
[40] K. Crane, U. Pinkall, and P. Schröder, "Robust fairing via conformal curvature flow," *ACM Trans. Graph.*, vol. 32, no. 4, pp. 1–10, Jul. 2013.
[41] M. P. Do Carmo, *Differential Geometry of Curves and Surfaces*. 2nd ed., New York, NY, USA: Dover, 2016.
[42] L. Wu, R. Falque, V. Perez-Puchalt, L. Liu, N. Pietroni, and T. Vidal-Calleja, "Skeleton-based conditionally independent Gaussian process implicit surfaces for fusion in sparse to dense 3D reconstruction," *IEEE Robot. Autom. Lett.*, vol. 5, no. 2, pp. 1532–1539, Apr. 2020.
[43] S. H. Sadati, Z. Mitros, R. Henry, L. Zeng, L. Da Cruz, and C. Bergeles, "Real-time dynamics of concentric tube robots with reduced-order kinematics based on shape interpolation," *IEEE Robot. Autom. Lett.*, vol. 7, no. 2, pp. 5671–5678, Apr. 2022.
[44] P. Rao, Q. Peyron, and J. Burgner-Kahrs, "Using Euler curves to model continuum robots," in *Proc. IEEE Int. Conf. Robot. Autom. (ICRA)*, May 2021, pp. 1402–1408.
[45] R. Levien, "The Euler spiral: A mathematical history," EECS Dept., Berkeley, CA, USA, Tech. Rep. UCB/EECS-2008–111, 2008.

Luhao Xie received the B.S. degree in instrument science and engineering from Hefei University of Technology, Hefei, China, in 2022. He is currently pursuing the Ph.D. degree with Jiangsu Key Laboratory of Robot Sensing and Control, School of Instrument Science and Engineering, Southeast University. His research interests include teleoperation, robotics, path planning, and their clinical applications.

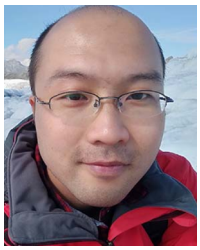

Lifeng Zhu (Member, IEEE) received the Ph.D. degree in computer science from Peking University, Beijing, China, in 2012. He is currently a Professor with the Department of Instrument Science and Engineering, Southeast University. His research interests include graphics, haptics, robotics, and their clinical applications.

Xiaoliang Jin (Member, IEEE) received the Ph.D. degree in intelligent mechanical systems engineering from Kagawa University, Takamatsu, Japan, in 2022. He is currently a Post-Doctoral Researcher with the State Key Laboratory of Digital Medical Engineering, Jiangsu Key Laboratory of Remote Measurement and Control, School of Instrument Science and Engineering, Southeast University, Nanjing, China. His research interests include medical robotics, force control, and haptic feedback.

Aiguo Song (Senior Member, IEEE) received the Ph.D. degree in measurement and control from Southeast University, Nanjing, China, in 1996.

From 1996 to 1998, he was an Associate Researcher with the Intelligent Information Processing Laboratory, Southeast University. From 1998 to 2000, he was an Associate Professor with the School of Instrument Science and Engineering, Southeast University. From 2000 to 2003, he was the Director of the Robot Sensor and Control Laboratory, Southeast University. From April 2003 to April 2004, he was a Visiting Scientist with the Laboratory for Intelligent Mechanical Systems (LIMS), Northwestern University, Evanston, IL, USA. He is currently a Professor with the School of Instrument Science and Engineering, Southeast University, and the Director of the Robot Sensor and Control Laboratory. He has published more than 400 peer-reviewed journal articles, and has received the Best Paper Award more than 30 times. His current interests concentrate on teleoperation robot, medical robot, space robot, and rehabilitation robot.

Dr. Song is a member of Chinese Instrument and Control Association and the Chair of the IEEE Nanjing Section Robotics and Automation Society Chapter. He is currently the chair or the co-chair of more than 60 international conference/symposium. He was a recipient of the second prize of the National Scientific and Technological Progress in 2017.